Carbon-13 magic angle spinning NMR study of the light-induced and temperature-dependent changes in Rhodbacter sphaeroides R26 reaction centers enriched in [4'-13C]tyrosine

Fischer, M.R.; Groot, H.J.M. de; Raap, J.; Winkel, C.; Hoff, A.J.; Lugtenburg, J.

^{13}C Magic Angle Spinning NMR Study of the Light-Induced and Temperature-Dependent Changes in *Rhodobacter sphaeroides* R26 Reaction Centers Enriched in [4′-^{13}C]Tyrosine†

M. R. Fischer,‡ H. J. M. de Groot,*,§ J. Raap,§ C. Winkel,§ A. J. Hoff,‡ and J. Lugtenburg§

Department of Biophysics, Huygens Laboratorium, and Department of Chemistry, Gorlaeus Laboratoria, Leiden University, P.O. Box 9502, 2300 RA Leiden, The Netherlands

Received February 4, 1992; Revised Manuscript Received July 16, 1992

ABSTRACT: Solid-state ^{13}C magic angle spinning (MAS) NMR has been used to investigate detergent-solubilized photosynthetic reaction centers of *Rhodobacter sphaeroides* R26, selectively enriched in [4-^{13}C]-tyrosine. The reaction centers were frozen, in the dark and while subject to intense illumination, and studied at temperatures between ~215 and ~260 K. The signal consists of at least seven narrow lines superimposed on a broad doublet. The chemical shift anisotropy is similar to that for crystalline tyrosine. The two narrowest resonances, corresponding to signals from individual tyrosines, are 28 ± 5 Hz wide, comparable to what is observed for quaternary carbons in linearly elastic organic solids. The line width as well as the chemical shift of these signals is essentially independent of temperature. This provides strong evidence for an unusually ordered, well-shielded, and structurally, electrostatically, and thermodynamically stable interior of the protein complex without structural heterogeneities. As the temperature is lowered, additional signal from the labels develops and the natural abundance resonances from the detergent broaden, providing evidence for considerable flexibility at the exterior of the protein complex and in the detergent belt at the higher temperatures. In addition, the NMR provides evidence for an electrostatically uniform and neutral complex, since the total dispersion in isotropic shifts for the labels is <5 ppm and corresponds to electron density variations of less than 0.03 electronic equivalents with respect to tyrosine in the solid state or in solution. When the sample is frozen while subject to intense illumination, a substantial part of the protein is brought into the charge-separated state $P^{\bullet+}Q_A^{\bullet-}$. At least three sharp resonances, including the narrowest lines, are substantially reduced in intensity. It is argued that this effect is caused by the electronic spin density associated with the oxidized primary donor $P^{\bullet+}$. These results strongly suggest that the environment of the special pair is extremely rigid and question the role of protein conformational distortions during the primary photoprocess.

The RC[1] of the photosynthetic bacterium *Rhodobacter sphaeroides* is a transmembrane protein complex that consists of three polypeptide chains (L, M, and H) and further contains four bacteriochlorophylls, two bacteriopheophytins, two quinones, and one Fe^{2+} ion. Following the pioneering work of Deisenhofer and Michel (1989), the complex has been crystallized, and its structure is now known in great detail (Rees et al., 1989; Chang et al., 1991). The cofactors form two nearly symmetric branches, denoted by A and B. The photochemistry involves the transfer of electrons from a bacteriochlorophyll dimer (P) at the periplasmic side of the RC over the A branch to the quinones, first Q_A and subsequently Q_B. The chlorophylls and pheophytins are supported by transmembrane helices of the L and M subunits in the only segment of the complex that is almost strictly nonpolar and rigid (Rees et al., 1989; Chang et al., 1991). The H-subunit is asymmetric and consists of one transmembrane helix and a large globular-type cytoplasmic domain (Rees et al., 1989; Chang et al., 1991).

Intensive study of RCs has provided detailed insight in the functional role of the prosthetic groups, their connection with electron pathways, and the time scales of various steps in the photochemistry [for a review, see, e.g., Friesner and Won (1989)]. Much less is known, as yet, about the functional role of the three polypeptide chains in the complex, and the mechanisms by which specific amino acids operate and contribute to symmetry breaking between the A and B branch, electron transport, and proton translocation.

Obviously, the most important function of the polypeptides is to provide the RC with its specific geometry and to support the cofactors. In addition, the protein is thought to establish an electrostatic potential that may help the charge separation and proton translocation (Yeates et al., 1987; Treutlein et al., 1988b; Parson et al., 1990). Conformational changes of the protein following excitation with light may be important for the photochemistry, while also rigidity of parts of the protein complex, in order to preclude such changes, may be essential for the function. X-ray data, hole-burning experiments, and molecular dynamics calculations provide only limited insight into these details of the structure–function relationship. The packing and Debye–Waller factors indicate a very rigid interior of the complex (Deisenhofer & Michel, 1989; Chang et al., 1991). Hole-burning experiments have been interpreted in terms of a strong coupling to low-energy protein conformational distortions during the primary photochemistry [see,

† This research was supported by the Netherlands Foundation for Chemical Research (SON) and the Netherlands Organization for the Advancement of Pure Research (NWO). H.J.M.d.G. is a recipient of a research career development fellowship (Akademie-Onderzoeker) from the Koninklijke Nederlandse Akademie van Wetenschappen (Royal Dutch Academy of Sciences).

* To whom correspondence should be addressed.
‡ Huygens Laboratorium.
§ Gorlaeus Laboratoria.

[1] Abbreviations: λ_{max}, absorption maximum, CP, cross-polarization; EPR, electron paramagnetic resonance; LDAO, *N,N*-dimethyldodecylamine-*N*-oxide; MAS, magic angle spinning; NMR, nuclear magnetic resonance; RC, reaction center; TMS, tetramethylsilane.

0006-2960/92/0431-11038$03.00/0

e.g., Johnson et al. (1991)]. In addition, molecular dynamics simulations have been performed in an attempt to map dynamic aspects on time scales up to ~100 ps in the transmembrane region of RCs (Parson et al., 1988; Creighton et al., 1988; Warshel et al., 1989; Treutlein et al., 1988a, 1992).

NMR is an excellent technique to probe the protein dynamics, structural heterogeneity, and local electrostatic effects. For proteins like the RC, with a molecular mass of more than 100 kDa, atomic selectivity can be obtained by using high-resolution CP/MAS NMR to study specifically enriched samples (de Groot et al., 1990a). This strategy allows the investigation, with atomic selectivity, of functionally active *unmodified* RC complexes, as distinct from site-directed mutagenesis studies. The method is sensitive to fluctuations at time scales between $\sim 10^{-2}$ and $\sim 10^{-10}$ s through the longitudinal and transverse relaxation times T_1 and T_2, the longitudinal relaxation in the rotating frame T_1^{ρ}, and the time scales associated with the chemical shift anisotropy and the heteronuclear dipolar interactions. Recently, we have succeeded in obtaining the first MAS NMR spectra with atomic selectivity from specifically labeled R26 RCs (de Groot et al., 1990a; Gephard et al., 1991). The purpose of the present study is to explore the microscopic electrostatic and rheological properties of the RC complex through their effect on the NMR signals of ^{13}C labels at the 4′ position of the phenolic side chain of the tyrosines. To this end, the NMR response and the nuclear relaxation properties were measured at various temperatures between 200 and 265 K, the range where freezing of different types of protein motion takes place (Brooks et al., 1988). In addition, data were taken on samples in which a substantial fraction of the primary donors was oxidized by freezing under intense illumination.

The R26 RC contains a total of 28 Tyr residues distributed over the complex (Williams et al., 1986), and therefore an overall impression of the variation of the electrostatic and dynamic properties throughout the protein is obtained. No evidence was found for substantial electrostatic effects associated with, for instance, nearby protein charges or differences in protonation states of the tyrosines. The data show that the interior of the complex is rigid, while considerable mobility appears to persist down to ~200 K at the surface of the complex. The NMR also provides unambiguous evidence that the protein surrounding of the special pair is a rigid entity that is static on the CP/MAS NMR time scale and is the most precisely defined section of the protein as probed by the labels, giving rise to very narrow resonances.

MATERIALS AND METHODS

Highly enriched (99%) [4′-^{13}C]tyrosine was synthesized as described in Winkel et al. (1989). The location of the label is indicated with an asterisk in the scheme at the top of Figure 2. Cells of *R. sphaeroides* R26 were grown in a synthetic medium containing the labeled tyrosine (Raap et al., 1990). For the isolation of reaction centers, the procedure of Feher and Okamura (1978) was used. Approximately 18 mg of the protein complex, embedded in detergent vesicles (LDAO, Fluka, Switzerland), was obtained. The [4′-^{13}C]Tyr incorporation in the complex was determined with mass spectrometry and is ~98% (Raap et al., 1990). The sample preparation procedure used in our laboratory yields purified protein complexes containing the Q_A cofactor. This is regularly checked with EPR. Q_B is largely removed due to the fairly high detergent concentration, in particular for the concentrated NMR samples.

CP/MAS NMR is the method of choice to obtain high-resolution NMR access to very large proteins (Griffin et al., 1988a; Smith & Griffin, 1988). Low-temperature 100-MHz ^{13}C CP/MAS NMR experiments were performed with a MSL-400 NMR spectrometer using a 7-mm MAS probe (Bruker, Karlsruhe, Germany). The spinning rate around the magic angle was kept at $\omega_r/2\pi = 5.00 \pm 0.01$ kHz with a spinning speed controller constructed in our laboratory (de Groot et al., 1988). The spectra were accumulated in up to 8K channels with ^{1}H decoupling during acquisition. The 90° pulse lengths for the ^{1}H and ^{13}C were 4–5 μs, the mixing time was 1 ms, the recycle delay 2 s, and the sweep width 50 kHz.

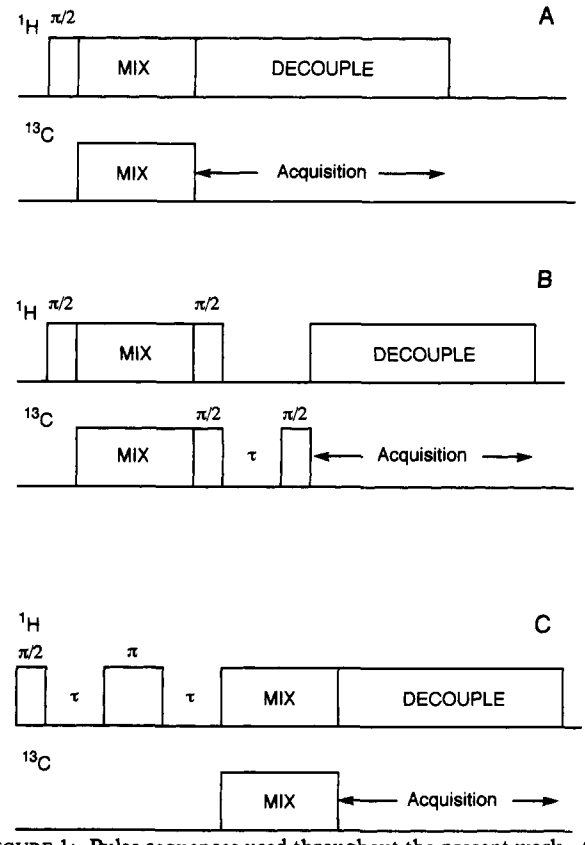

FIGURE 1: Pulse sequences used throughout the present work. (A) ^{1}H–^{13}C cross-polarization with acquisition under continuous proton decoupling. (B) ^{1}H–^{13}C cross-polarization followed by a ^{13}C inversion–recovery T_1 scheme with delay time τ. (C) Sequence to measure the defocusing of the proton magnetization due to T_2-type relaxation processes, with a refocusing π-pulse to correct for resonance offset, and ^{1}H–^{13}C cross-polarization prior to ^{13}C detection.

The pulse sequences used for this study are shown in Figure 1. Figure 1A is the CP scheme originally proposed by Tegenfelt and Haeberlen, (1979), without the flip-back pulse, which was unnecessary since the proton T_1 of the RC complex is short (~100 ms at 260 K and ~1 s at 200 K). The pulse scheme in Figure 1B was used to perform an inversion–recovery T_1 measurement. The ^{13}C magnetization is turned opposite to the direction of the applied magnetic field with a $\pi/2$ pulse immediately after cross-polarization, allowed to recover during a time τ, and probed with another ^{13}C $\pi/2$ pulse. The sequence of Figure 1C provides information about the T_2 of the proton magnetization, which evolves after a $\pi/2$ pulse during a time τ, is refocused with a π pulse, and detected with the ^{13}C resolution after the same τ through cross-polarization to the ^{13}C nuclei (Harbison et al., 1988).

The tyrosine signals were separated from the natural abundance background by subtracting a spectrum recorded with the same spinning speed from a natural abundance R26 sample at the same temperature (de Groot et al., 1988). The resulting difference spectrum was deconvoluted with Lorent-

zian lines, with the first and second derivatives of the signal included in the analysis in order to give appropriate weight to small peaks and shoulders. Chemical shift anisotropies were calculated with the Herzfeld–Berger Method (Herzfeld & Berger, 1980), using the CERN (Geneva) MINUIT fitting package (de Groot et al., 1991). For the interpretation of the results, extensive use was made of the coordinate data sets of Rees et al. (1989) and Chang et al. (1991) and the TURBO-FRODO display program (Bio-Graphics, Marseille, France). The calculations and displaying were done on a Personal Iris 4D35 workstation (Silicon Graphics Inc., Mountain View, CA).

In order to immobilize the detergent-solubilized protein complex, the samples were frozen using liquid nitrogen cooled bearing gas. The equipment for cooling the gas is described in Allen et al. (1991). The temperature of the gas T_B was varied with a heater in the probe. In the CP/MAS probe, T_B is measured just before the gas enters the stator. The actual sample temperatures are higher and depend slightly on the amount of drive gas, which was kept at ambient temperature. A reasonable estimate for the sample temperature T, accurate to about 5 K, is obtained with the relation $T \sim 0.86T_B + 50$ (H. Förster and A. C. Kolbert, unpublished results).

At moderately low temperatures, $T \sim 200$ K, a large fraction of the RC complexes, up to ~80% for a dilute sample, can be maintained in the $P^{\bullet+}Q_A^{\bullet-}$ state if the sample is kept under continuous illumination, both while freezing it and while doing the NMR experiment. In our studies, we are only concerned with the oxidized primary donor $P^{\bullet+}$, since the effect of spin density on the acceptor can be neglected (vide infra). To generate $P^{\bullet+}$, we used a 300-W xenon light source (ILC Technology, Sunnyvale, CA). The light was transported through a commercial liquid-filled light guide (Ultrafine Technology, Great Britain) and a plexiglass rod fixed in the MAS probe terminating at a distance of ~2 mm from the translucent Kel-F cap of the rotor. Using this setup, the sample can be illuminated over a broad spectrum 400 nm $< \lambda <$ 800 nm with high intensity. The illumination was tested in an E9 EPR spectrometer from Varian (Palo Alto, CA) by monitoring the light-induced primary donor signal of a ~1.5-mm thick sample with approximately the same optical density as the NMR sample and ~50% conversion was easily achieved. For the NMR experiments on the labeled protein, a half-filled rotor was used. The sample was frozen under intense illumination, while slowly spinning ($\omega_r/2\pi \sim 400$ Hz) to ensure that the major part of the reaction centers was spread against the rotor wall in a ~1.5-mm thick layer and stirred by the rotation while freezing the sample.

A control experiment was performed following a different procedure. A small translucent Kel-F sample holder that fits tightly into the NMR rotor was filled with labeled protein and frozen to ~180 K with cooled N_2 gas in a quartz flow-cryostat under continuous sideways illumination from a 1000-W Aldis projection lamp in the EPR spectrometer. A water filter (thickness ~ 5 cm) was used for IR cut-off. The oxidized primary donor EPR signal was monitored during cooling, and the estimated conversion was again ~50%. Turning off the light at temperatures around 200 K yielded after a few minutes an almost constant signal of ~75% of the original EPR signal intensity. The sample was put in liquid nitrogen, inserted in an NMR rotor, and transferred to the MAS probe, which was rapidly cooled to ~210 K in about 1 min. The effects on the NMR spectrum, collected in the dark, were less pronounced than the effects on the spectrum observed after in situ illumination. The sample was taken to the EPR spectrometer, while keeping it cold, and then measured at ~180 K. Again an oxidized primary donor signal was observed, at ~30% of the original intensity. After the sample was thawed, adapted in the dark for 10 min, and then refrozen in the dark, the EPR signal had disappeared. Subsequent ^{13}C NMR showed the reappearance in the CP/MAS spectrum of the sample before the illumination experiment. This shows that the light-induced changes in the RC detected with the CP/MAS NMR are reversible.

The presence of localized electronic spins strongly affects the relaxation properties of ^{13}C nuclei. The effects on the T_1, the T_1^ρ, and the T_2 are of importance for the interpretation of the NMR data obtained in the present study. The direct effect, neglecting spin diffusion, of a paramagnetic center with correlation time τ_p, gyromagnetic ration γ_p, and spin S on the T_1 of the a nucleus at a distance r, with gyromagnetic ratio γ_n, and resonating at a frequency $\omega_0/2\pi$ may be approximated as (Lowe & Tse, 1968; Devreux et al., 1974)

$$T_1^{-1} \simeq \frac{2\gamma_p^2 S(S+1)\gamma_n^2\hbar^2}{5}\left[\frac{\tau_p}{1+\omega_0^2\tau_p^2}\right]r^{-6}$$

while

$$T_1^{\rho-1} \simeq \gamma_p^2 S(S+1)\gamma_n^2\hbar^2\left[\frac{4}{15}\frac{\tau_p}{1+\omega_1^2\tau_p^2}+\frac{1}{5}\frac{\tau_p}{1+\omega_0^2\tau_p^2}\right]r^{-6}$$

where ω_1 measures the spin-lock field strength. For an estimate of the T_2 broadening, of the individual center band and side bands that contribute to the MAS pattern, eq 24 of Suwelack et al. (1980) was used, with the electronuclear dipolar coupling for a $S = {}^1/_2$ electronic magnetic moment instead of the chemical shift anisotropy:

$$T_2^{-1} \simeq \frac{1}{15}\gamma_p^2\gamma_n^2\hbar^2\left[\frac{\tau_p}{1+4\omega_r^2\tau_p^2}+\frac{2\tau_p}{1+\omega_r^2\tau_p^2}\right]r^{-6}$$

It transpires that the T_1, T_1^ρ, and T_2 are sensitive to fluctuations of different frequencies, T_1 is mainly shortened if $\omega_0\tau_p \approx 1$, T_1^ρ if $\omega_1\tau_p \approx 1$, and T_2 if $\omega_r\tau_p \approx 1$. In our experiments, $\omega_0 = 6.3 \times 10^8$ rad/s (^{13}C) or $\omega_0 = 2.5 \times 10^9$ rad/s (^1H), $\omega_1 = 4 \times 10^5$ rad/s, and $\omega_r = 3 \times 10^4$ rad/s.

In order to characterize the small changes in the line shape of the tyrosine signal induced by light and variation of the temperature, a good calibration of the chemical shift, given relative to TMS, is indispensable. Thermal contractions associated with the cooling of the probe affect the calibration of the chemical shift by ~1 ppm. The resonance at 14.4 ppm from the ^{13}C-12 of the LDAO remains narrow at low temperatures (cf. Figure 2) and was used as an internal calibration. To ensure that there are no spurious shifts of downfield resonances between different spectra, all data taken with the pulse scheme of Figure 1A were recorded with the same dead time of 10 μs, and the first-order phase correlation after Fourier transformation was always kept at the same small value of 25° for these spectra. The calibration was also checked regularly against the two natural abundance ^{13}C resonances in a sample of solid crystalline glycine. The data obtained with the sequences of Figure 1, panels B and C, were calibrated against data sets obtained with the scheme of Figure 1A, at the same temperatures. In this way, the absolute error in the chemical shift could be reduced to ~0.2 ppm.

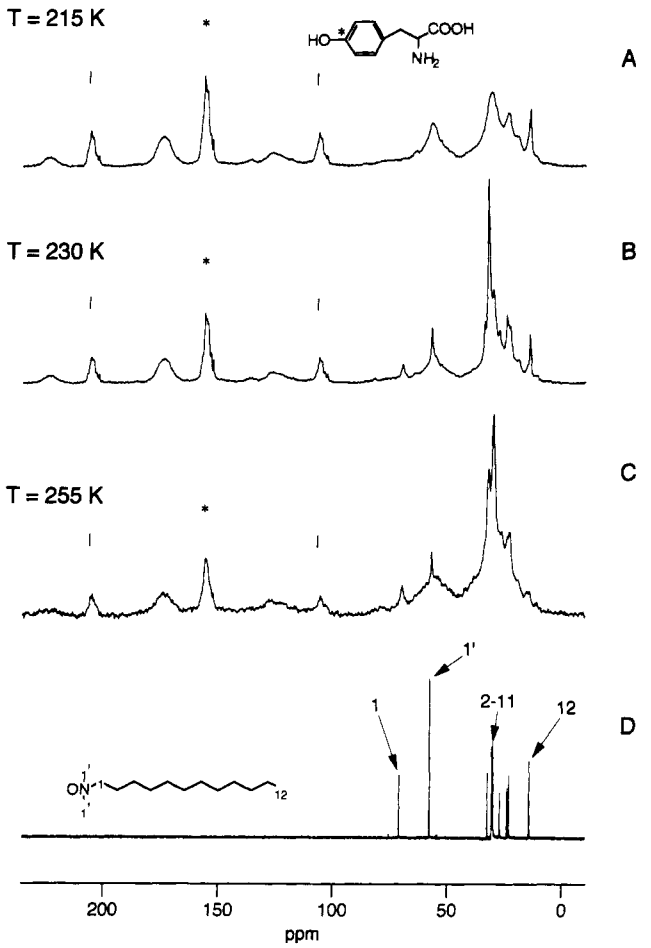

FIGURE 2: Proton-decoupled ^{13}C CP/MAS spectra for [4'-^{13}C]Tyr R26, collected with a spinning speed $\omega_r/2\pi$ = 5.00 kHz at T = 215 K (A), 230 K (B), and 255 K (C). (D) The 75 MHz natural abundance ^{13}C spectrum of LDAO in a D_2O/H_2O mixture at ambient temperature. The position of the label is indicated (*) in the tyrosine scheme at the top of the figure. In panels A, B, and C, the center bands and side bands of the contributions from the label are indicated with an asterisk (*) and a vertical bar (|), respectively. The assignment of the detergent signals is indicated in panel D.

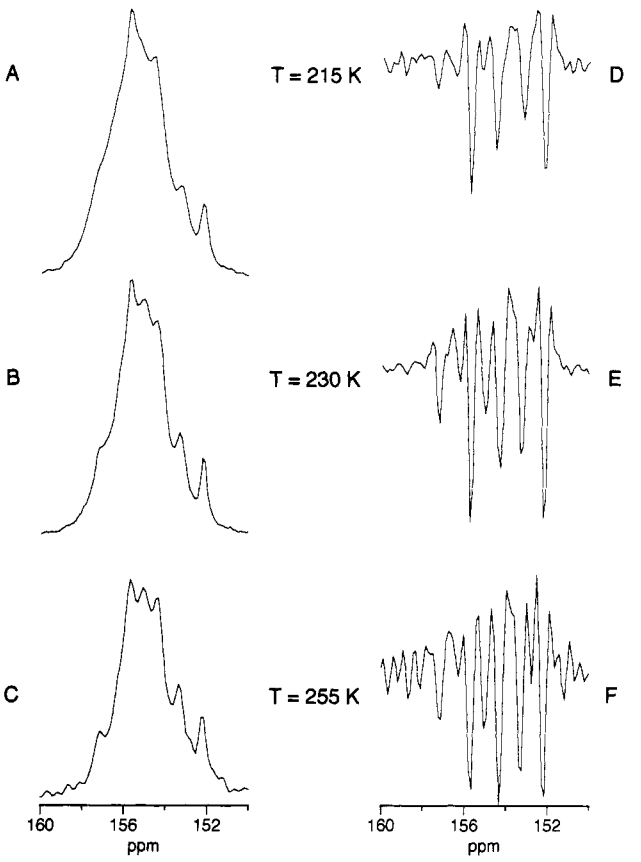

FIGURE 3: Center-band regions (left) and their second derivatives (right) of the contribution of the [4'-^{13}C]Tyr label to ^{13}C CP/MAS spectra of the R26 protein complex, collected with $\omega_r/2\pi$ = 5.00 kHz at T = 215 K (A, D), 230 K (B, E), and 255 K (C, F).

RESULTS

At room temperature, the ^1H–^{13}C dipolar interactions are cancelled on the time scale necessary for the cross-polarization (1–3 ms), since the RCs are detergent solubilized and are subject to rapid isotropic motion. The complexes can be immobilized by freezing. The transition occurs for $T \sim 265$ K and is easily detected since the ^1H tuning characteristics of the probe change.

Figure 2 shows the CP/MAS NMR spectra of the [4'-^{13}C]Tyr R-26 RCs in the frozen state at $T \sim 215$, 230, and 255K. In these spectra, three regions can be distinguished. Around 155 ppm the strong center-band resonances from the Tyr labels appear, indicated by an asterisk. The corresponding side bands at 105 and 205 ppm are indicated with vertical dashes. Upfield, between 0 and 70 ppm, the ^{13}C natural abundance background resonances from the aliphatic carbons is found. At temperatures just below the freezing point, the natural abundance background signal of the detergent molecules contributes a set of narrow center-band resonances (cf. Figure 2C). As the temperature is lowered, these signals, at 71.3 (^{13}C-1), 58.0 ($^{13}CH_3$), 31.2, ~24.0 (^{13}C-2–^{13}C-11), and 14.4 (^{13}C-12) ppm, increase and broaden in this order (Figure 2A,B). The assignments were obtained from a comparison with the solution spectrum of Figure 2D. At ~175 ppm, the center band of the natural abundance carbonyl resonances is observed, with its side bands around ~125 and ~225 ppm.

The center-band resonances of the tyrosine labels at temperatures $T \sim 215$, 230, and 255 K are plotted in Figure 3A–C. The line shape is temperature-dependent. Additional intensity evolves predominantly at the downfield side of the resonance as the temperature is lowered. The signal contains a variety of narrow peaks and shoulders, superimposed on a broader line. It was verified that the small features reproduce, by collecting various datasets, on two different samples. From the second-derivative spectrum in Figure 3F, it may be concluded that already at $T \sim 255$ K at least four narrow resonances are observed that remain well resolved and similarly strong in the second-derivative spectra at lower temperatures (Figure 3, panels D and E). Although the labeled carbons have no protons directly bonded, which may in principle reduce their cross-polarization efficiency, the signal appears to be essentially complete when using a contact time of 1 ms, as for the spectra of Figure 3. To illustrate this, data taken with a contact time of 4 ms are shown in Figure 4. Since the contact time is now beyond the CP optimum, there is less signal intensity, and apparently the broader features exhibit the shortest T_1^ρ. However, it is clear from the second-derivative spectrum in Figure 4B that there are no new strong sharp resonances in addition to the four that were already present in the spectra taken with a contact time of 1 ms.

In terms of signal-to-noise and resolution, the best spectrum is observed at $T \sim 250$ K (Figures 2B and 3B). For the signals at 152.2 and 155.7 ppm, any variation of the shift or the line width in the three spectra is less than the resolution (0.1 ppm). The two other distinctive signals, at 153.4 and 153.9 ppm, are slightly temperature dependent. Both show

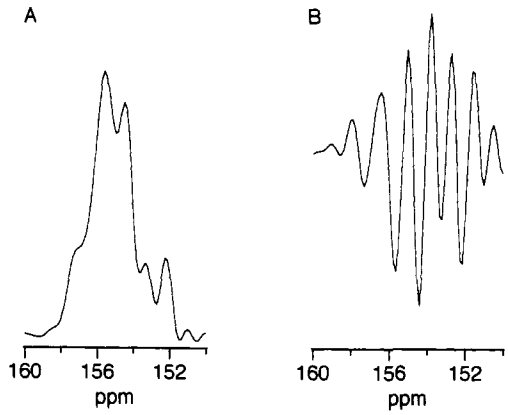

FIGURE 4: Center-band region (A) and its second derivative (B) of the contribution of the [4′-^{13}C]Tyr label to a spectrum collected with a cross-polarization time of 4 ms at $\omega_r/2\pi$ = 5.00 kHz and $T \sim 255$ K.

minor broadening at $T \sim 215$ K, and the line at 153.4 ppm shifts downfield when the temperature is lowered, but only by a very small amount of ~0.2 ppm. The principal components of the chemical shift anisotropy tensor were determined from the integrated intensities for the center bands and side bands of the two broader components as σ_{11} = 60(3) ppm, τ_{22} = 160 (40) ppm, and τ_{33} = 254 (3) ppm, which translates[2] into an asymmetric anisotropy with δ = –9800 (300) Hz and $\eta \sim 1$, in agreement with our previous work (de Groot et al., 1990a). For the four narrow resonances that are well-resolved in all second-derivative spectra, it could be verified through a computer analysis (see below) that the principal components of the σ tensor are similar to those for the broader resonances, while for the remaining smaller features the σ components were assumed to be the same throughout the analysis.

Figure 5 shows the result of the CP/MAS inversion–recovery experiments with the pulse scheme of Figure 1B, performed at $T \sim 255$ K. The spin–lattice relaxation times for the label and the natural abundance carbonyl resonances are quite long ($T_1 > 1$ s). No substantial differences in T_1 between the various tyrosines are observed at this temperature, since the overall shape of the tyrosine center band remains the same for all τ values. The T_1's of the detergent signals are short and are estimated as ~60 ms (1′-^{13}C), ~0.1 s (1-^{13}C), ~0.3 s (2-11-^{13}C's), and ~0.5 s (12-^{13}C).

In Figure 6 a series of spectra obtained with the sequence of Figure 1C at $T \sim 260$ K is shown. This experiment is meant to probe the decay of the polarization due to T_2-type relaxation of the protons in the immediate vicinity of the ^{13}C nuclei observed in these spectra (Harbison et al., 1988). It appears that the tyrosine label and detergent resonances are still discernable in the τ = 500 μs spectrum, while the carbonyl signals (~175 ppm) and the broad background in the aliphatic region (0–70 ppm) decay rapidly. The same experiments were performed at a lower temperature $T \sim 230$ K. In addition, we measured the T_2 of a narrow proton resonance, which is attributed to a mobile fraction of water molecules or hydrogen-bonding protons in the sample below the freezing point.

A selection of the results of these protons T_2 selective experiments is summarized in Figure 7, which shows the variation of the signal intensity versus total decay time $2\tau + \tau_{180}$ for the tyrosine labels, the carbonyls, and the 1′-^{13}C of the detergent. Here τ_{180} = 10 μs is the π pulse length for the protons. The characteristic decay times estimated from the

[2] Calculated as $\delta = (\sigma_{11} - \sigma_i)/(\omega_0/2\pi)$, with $\omega_0/2\pi$ = 100 MHz, the ^{13}C NMR frequency, and $\eta = (\sigma_{22}-\sigma_{11})/\sigma_{33}$.

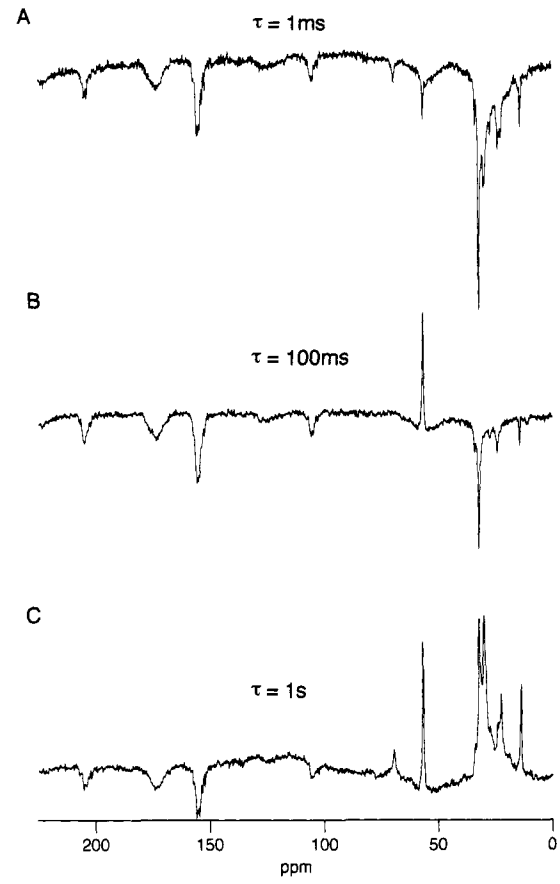

FIGURE 5: CP/MAS inversion–recovery data for the [4-^{13}C]Tyr R26 protein complex obtained with the pulse scheme of Figure 1B with τ = 1 ms (A), 100 ms (B), and 1 s (C), at a temperature T = 255 K with a spinning speed $\omega_r/2\pi$ = 5.00 kHz.

slopes of these curves are listed in Table I. The carbonyl signal disappears within ~50 μs at both temperatures while the decay of the 1′-^{13}C of the LDAO is an order of magnitude slower at 260 K. The decay of the tyrosine peak with τ is clearly nonexponential. At both temperatures, for $\tau < 40$ μs the signal decreases with a rate similar to that of the carbonyl signal at that temperature, whereas the remaining part relaxes at the time scale of the detergent signal.

Previous studies on photobiological pigments have shown that it is possible to perform CP/MAS NMR on frozen intermediates (Smith et al., 1989, 1991), provided that the sample is illuminated with light of a broad spectrum to ensure deep penetration of the light into the optically dense NMR sample. In this work, the samples were illuminated in the spectral range 400–800 nm where the absorption is lowest. The absorbed photons excite the primary donor bacteriochlorophyll dimer P (λ_{max} = 865 nm) by direct excitation or energy transfer. $P^{\bullet+}$ was stabilized by freezing the sample in a slowly turning MAS rotor under intense illumination. The center band of the resonance from the labels in the CP/MAS NMR spectrum of illuminated [4′-^{13}C]tyrosine-R26 reaction centers at T = 215 K is shown in Figure 8A and compared with a spectrum of the same sample obtained in the dark. The precise criteria for the relative scaling of these two data sets are discussed below. The first and second derivatives of these spectra are shown in Figure 8, panels B and C, respectively. In the presence of $P^{\bullet+}$, a different line shape is observed, and several of the sharp resonances appear to be partially suppressed with respect to the signal of the complex in the dark.

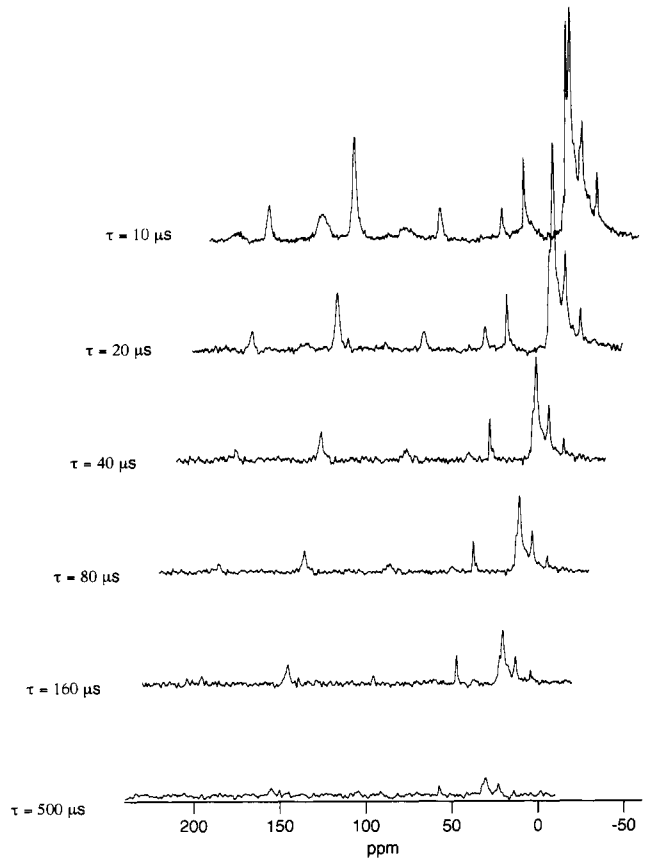

FIGURE 6: Proton T_2 selective CP/MAS data for the [4′-^{13}C]Tyr R26 protein complex obtained with the pulse scheme of Figure 1B with various delay times at a temperature T = 260 K and with a spinning speed $\omega_r/2\pi$ = 5.0 kHz.

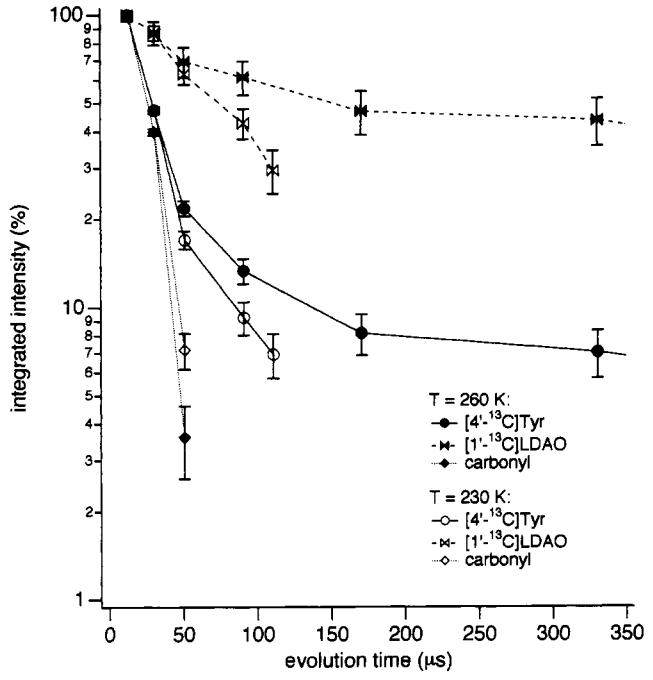

FIGURE 7: Integrated intensities of the label signals versus total evolution time for various resonances in the proton T_2 selective experiments at T = 230 K (open symbols) and T = 260 K (filled symbols). The lines are guides to the eye.

DISCUSSION

In-depth insight in the electrostatic, dynamic, and thermodynamic properties of the protein will help to understand its functional role. The MAS NMR experiments on the specifically labeled samples enable us to probe electrostatic differences and structural heterogeneity through the dispersions of the isotropic shifts and the line widths, while examining the cross-polarization efficiency, line shape, chemical shift anisotropy, and relaxation properties renders detailed information about the dynamics. By specific labeling of the tyrosine, it is possible to probe the protein complex on 28 geometrically known locations, with additional information coming from the natural abundance background signals of the protein and the detergent molecules that form the vesicles around the complex. Illumination with light creates paramagnetic centers that strongly affect the NMR signals and permits a further characterization of the environment of the special pair.

NMR Evidence for Rigid and Spectroscopically Well-Defined Sections of the Complex. It is known that membrane proteins can yield strong cross-polarization signals, even at ambient temperature, provided that the protein or complex is not subject to rapid rotational diffusion (Lewis et al., 1985; Harbison et al., 1985). The tyrosine signal at $T \sim 255$ K, just below the freezing point, already contains at least four narrow lines. The tyrosines associated with these signals should be located in a rigid section of the protein. A deconvolution of the label signal at $T \sim 230$ K reveals small peaks at 152.2, 153.9, 154.4, 155.1, 155.7, 156.9, and 157.3 ppm that are also well resolved in the second-derivative spectrum of Figure 3E and possibly one at 156.3 ppm (Figure 9). The line widths are ~30 Hz and are mainly limited by the intrinsic resolution

Table I: Estimated Proton T_2 Times

	T = 230 K (μs)	T = 260 K (μs)
[4′-^{13}C]tyr (fast)[a]	20	20
[4′-^{13}C]tyr (slow)[a]	60	700
[1′-^{13}C]LDAO[a]	80	500
^{13}C carbonyl[a]	20	20
H_2O[b]	200	700

[a] Measured with the pulse scheme of Figure 1C. [b] Measured directly with a standard echo sequence.

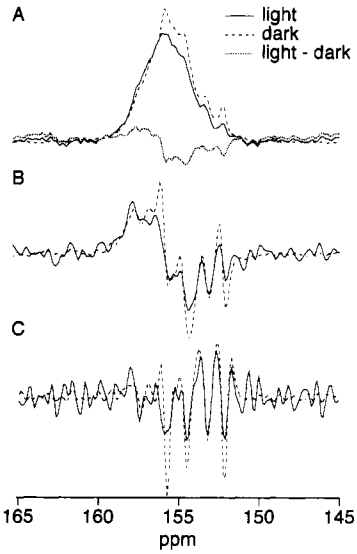

FIGURE 8: Center-band regions of the signals from the [4′-^{13}C]Tyr labels to ^{13}C CP/MAS difference spectra (T = 215 K, $\omega_r/2\pi$ = 5.0 kHz) of the R26 protein complex in the light-induced, partially charge-separated state P^+Q^- (solid lines) and the relaxed state in the dark (dashed lines). (A) Difference spectra and (B) first and (C) second derivatives. In panel A, the (double) difference between the light and dark signals is also shown (dotted line).

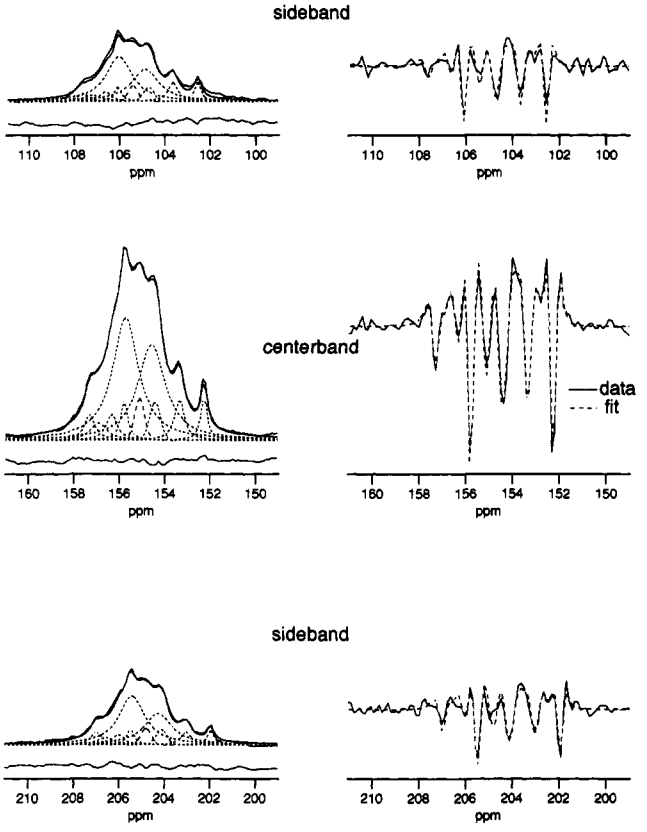

FIGURE 9: Deconvolution of the center band and first two side bands from the [4′-^{13}C]Tyr resonances in the ^{13}C CP/MAS difference spectrum with $\omega_r/2\pi$ = 5.0 kHz, obtained from the spectrum of Figure 2 with T = 230 K, by subtracting a natural abundance spectrum collected at the same temperature and spinning speed (not shown). In the left part the data and fit are depicted by solid lines, while the individual components that contribute to the fit are dashed. Below each band, the residue after analysis, data minus fit, is shown. The right part shows the second derivatives of data (solid line) and fit (dashed line).

of the ^{13}C CP/MAS experiment. The intensities vary between 3.5% and 5% (with a statistical error of ~1%) of the total intensity of the resonance from the label, and therefore the small contributions should correspond to resonances from individual tyrosines in the protein complex. The remaining intensity is divided over two broader signals around 155.7 and 154.5 ppm. The two narrowest components resonate at 152.2 and 155.7 ppm. Their shifts are practically independent of temperature and both exhibit a width of 28 ± 5 Hz down to 230 K. This is unusual, since ^{13}C resonances of proteins are normally subject to some inhomogeneous broadening when the temperature is lowered. For instance, slight broadening at low temperatures has been observed in the ^{13}C NMR of the retinylidene prosthetic group in the interior of the membrane protein bacteriorhodopsin (de Groot et al., 1990b). This has been attributed to small heterogeneities, for instance, structural heterogeneities that generally occur when the sample is cooled and frozen into multiple conformational substates or contained in a glassy ice matrix that exerts stress and pressure on the protein (Frauenfelder & Wolynes, 1985; Brooks et al., 1988). The signals at 152.2 and 155.7 ppm do not exhibit any detectable line broadening upon cooling. Hence they originate from sections of the complex that are very well shielded from external stress. In addition, the chemical environment of the tyrosines associated with these signals is unique, and extremely well-defined, structurally, electrostatically, and thermodynamically.

Since the cross-polarization for the four narrow signals that dominate the second-derivative spectra is already quite efficient at the highest temperatures and the principal components of their σ tensors closely resemble those of crystalline [4′-^{13}C]-tyrosine (Pausak et al., 1973; Veeman, 1984), it follows that the tyrosine side chains associated with these signals are static on the CP/MAS NMR time scale. Rapid [$\tau_c \leq (2\pi\delta)^{-1} \sim 30\ \mu s$] rotational diffusion of the tyrosine ring over more than ~20°, would give rise to (partial) incoherent averaging of the σ_{22} and σ_{11} components of the chemical shift anisotropy, which are directed in the plane of the ring perpendicular to the C–O bond and perpendicular to the plane of the ring, respectively (Pausak et al., 1973). In addition, diffusive tyrosine ring rotation should give rise to an excess linewidth $\Gamma_e = (\pi T_2)^{-1}$ of the MAS pattern where[3] $T_2^{-1} \sim (9/80)[2\pi\delta\omega_r^{-1}(1 - \eta/3]^2\tau_c^{-1}$ (Suwelack et al., 1980). Since $\omega_r/2\pi$ is of the same order as δ in our experiments, and the principal components of the chemical shift anisotropy closely resemble the values obtained for crystalline tyrosine, the phenolic side chains that give rise to the narrow signals are obviously in the slow diffusion limit $\omega_r\tau_c \gg 1$. From our data, we deduce that any excess line width due to side-chain mobility amounts to less than 5 Hz for the two narrowest NMR resonances, yielding $\tau_c > 10^{-2}$ s at least. This agrees with available information about phenolic side-chain mobility in the interior of proteins. Often the motion appears to be low-frequency instantaneous ring flips with activation energies ~0.5 eV, high compared with the thermal energy $k_BT \sim 0.02$ eV (Campbell et al., 1976; Griffin et al., 1988b). The NMR of the 4′-^{13}C nucleus is not sensitive to instantaneous 180° ring flips that leave the symmetry in the protein and its conformation unaffected, since the chemical shift tensor of the 4′-^{13}C is mapped onto itself.

Some indication about the rheology of the complex can be obtained from the above data. There exists considerable evidence that microscopic correlation times can be roughly related to the viscosity of the medium using a crude Einstein–Stokes approximation (Zager & Freed, 1982). Hence a lower limit for the local viscosity $\eta_i \sim (3k_BT\tau_c)/(4\pi r_{Tyr}^3)$ around the phenolic side chains can be estimated. At temperatures T = 200–300 K, with r_{Tyr} = 1.5 Å and $\tau_c > 10^{-2}$ s, we calculate $\eta_i > 10^6$ Pa·s for the tyrosine labels associated with the two narrowest resonances (1 Pa·s = 10 Poise). This may be compared with, for instance, ~1 Pa·s for the viscosity of a lipid bilayer (Fischer & Stoeckenius, 1983), 10^5 Pa·s for molten polyethylene (Philippoff & Gaskins, 1956), and $>10^7$ Pa·s for a small organic molecule in the solid state (Weast & Astle, 1980). For viscosities as low as 1 Pa·s, materials already become detectably rigid and also exhibit elastic behavior (Van Wazer et al., 1963). Since the narrowest resonances have line widths typical for quaternary carbons in crystals of small organic molecules, i.e., linearly elastic solids, our data provide strong evidence for an elastic rather than viscous type of environment for these tyrosines.

Inspection of the X-ray data can help in finding residues that may be responsible for the narrow lines. Eleven hydrophobic helices of the L, M, and H subunits form a transmembrane framework that supports the cofactors, while four shorter helices span the cytochrome binding site, over the special pair. Together with the accessory chlorophylls and pheophytins, they shield an important section of the complex from the detergent, etc. This section contains eight tyrosines: L128, M198, and M210 inside the apolar transmembrane

[3] Equation 28 of Suwelack et al. (1980), with $\delta\eta$ replaced by $\sigma_{11}-\sigma_{22} = (3/2)\delta[1 - (1/3)\eta]$.

region, L148, L162, L169, and M177 toward the polar periplasmic side surface of the complex, and finally L222 in the Q_B binding domain at the cytoplasmic side of the transmembrane region (Rees et al., 1989; Chang et al., 1991).

Evidence for Mobility of the Detergent Belt and the Surface of the RC Complex. Motion at the surface and internal movements induced or mediated by the surface mobility may persist down to ~200 K [see, e.g., Brooks et al. (1988) and Parak et al. (1990)]. For the RC, this is most obvious from the temperature dependence and relaxation properties of the natural abundance background signal of the detergent, which forms a belt around the apolar transmembrane region (Roth et al., 1989). At temperatures just below the freezing point, the detergent molecules contribute a set of narrow center-band resonances (cf. Figure 2C). The T_1 relaxation, which is sensitive to fluctuations on the NMR time scale of $\omega_0/2\pi$ = 100 MHz, is relatively fast, $T_1 < 1$ s. At $T = 255$ K the cross-polarization is not very efficient, and the ^{13}C-12 resonance is not observed (Figure 2C). Apparently, the polar headgroups immobilize first, whereas the motion of the apolar chains freezes at lower temperatures. The strong and narrow lines from the detergent between $T = 230$ K and $T \sim 255$ K (Figure 2B) provide evidence for rotational diffusion that is fast compared to the chemical shift anisotropy $|\delta| = 10^3$–10^4 Hz. The motion is probably anisotropic around the apolar chain axis since reasonable ^{1}H–^{13}C cross-polarization efficiency is observed, indicating only partially quenched ^{1}H–^{13}C dipolar interactions. For the rapid diffusive rotation limit $\omega_r\tau_c \ll 1$, the $T_2^{-1} \sim (3/20)[2\pi\delta(1 - \eta/3)]^2\tau_c$ (Suwelack et al., 1980). With the excess line broadening argument used before, applied to the fast limit, it is calculated that $\eta_d \lesssim 10^2$ Pa·s for the detergent belt at this temperature.

Less than half of the protein complex comprises the membrane-spanning region that is expected to be rigid and should give rise to strong CP/MAS signals at any temperature below the freezing point of the buffer (Rees et al., 1989; Chang et al., 1991). The increase of the broad component at the downfield side of the label signal upon freezing involves residues which are not shielded and subject to heterogeneities, i.e., tyrosines that are exposed or otherwise influenced by the external stress on the complex. Experiments in this and other laboratories have shown that surfaces of larger proteins may not cross-polarize well down to ~230 K (Abrahams, 1991). To date, the most detailed X-ray data available are for the homologous RC of *Rhodopseudomonas viridis*. In this protein complex, tyrosine side chains with poor β factors > 20 are invariably associated with exposed residues (Deisenhofer & Michel, 1989). From the *R. sphaeroides* X-ray structure, it is possible to identify 13 residues with largely exposed phenolic side chains: L67, L73, L144, M76, M101, and M295 on the polar periplasmic side, L115, M51, M134, H29, and H30 on the transmembrane helices in the transition region between the apolar transmembrane section and the polar cytoplasmic domain, and H259 on the cytoplasmic domain of the H-subunit. In addition, most of the remaining tyrosines that are not exposed but outside the helix-shielded region (L9, L30, L164, M3, H40, H236, and H243) are located in polar segments of the complex. Only one exposed residue, H18, is on the apolar surface of the transmembrane section (Rees et al., 1989; Chang et al., 1991). This strongly suggests that the increase of the downfield side of the label resonance upon cooling is mainly associated with residues in a polar sections, in agreement with inferences in the previous work (de Groot et al., 1990a).

In the solid state, the proton T_2 is usually of the order of ~10 μs due to the strong ^{1}H homonuclear dipolar interactions (Abragam, 1961). The decay times of the natural abundance background carbonyl signal and the rapidly decaying component of the signal from the labels, as measured with the proton T_2 selective experiments at $T \sim 230$ K and $T \sim 260$ K (Figure 7 and Table I), are typical for a rigid environment. The slower component of the Tyr signal indicates that the protons in the immediate environment of some of the labels have a much longer $T_2 \sim 0.7$ ms, of the same order of the detergent headgroup and the slow component in the ^{1}H signal of the buffer. The chemical shift anisotropy of this slowly decaying component is again similar to the anisotropy of the 4'-^{13}C resonance in solid tyrosine. Together with the observation of a long T_1 for the labels this argues against rotational diffusion of the Tyr side chains associated with these CP/MAS signals as an underlying mechanism for the longer decay time. In earlier studies, similar effects have been attributed to rapid proton exchange around exposed or accessible residues (Harbison et al., 1988; M. Engelhard, unpublished results). This would explain why the slower component of the label signal at 230 K comprises additional intensity that evolves at the downfield side of the resonance when cooling.

Light-Induced Effects on the Tyrosine Resonances. The presence of a localized electronic spin strongly affects the CP/MAS signal of the ^{13}C nuclei in the immediate environment. Line broadening associated with shortening of T_1 or T_2 beyond ~10 ms may arise from the rapid fluctuations of the electronic moments that are communicated to the nuclei through the electronuclear dipolar interaction, while shortening of the T_1^ρ by the same interaction beyond ~1 ms will suppress the cross-polarization. In addition, the dipolar field from the paramagnetic moment can, in principle, affect the relative intensities of the side bands and center band of the MAS pattern. ENDOR data indicate that contact hyperfine contributions to the interaction of $P^{\bullet+}$ and the 4'-^{13}C nuclei associated with delocalization are unimportant as almost all unpaired spin density resides on the oxidized special pair (Feher et al., 1975; Möbius et al., 1989).

In order to interpret the effects of these paramagnetic moments on the NMR, it is necessary to know their correlation times τ_p. The RC in the dark contains a high-spin Fe^{2+} paramagnetic center (Debrunner et al., 1975). Mössbauer spectroscopy data reveal a quadrupole doublet characteristic for a rapidly fluctuating iron moment down to 4.2 K (Boso et al., 1981). In the motional narrowing regime, the excess Mössbauer line width due to paramagnetic fluctuations is $\Delta\Gamma \sim 2(^1/_4\omega_0^g + {}^3/_4\omega_0^e)^2\tau_p$ (de Groot, 1986), with ω_0^g and ω_0^e the nuclear Larmor frequencies of the ^{57}Fe ground and excited states, respectively, in the hyperfine field of the paramagnetic moment, which was estimated to be 17.5 T (Boso et al., 1981). Since no excess Mössbauer line broadening from slow paramagnetic fluctuations is observed down to 4.2 K, it follows that $\tau_p \lesssim 10^{-9}$ s at 4.2 K, so $\tau_p \ll 10^{-9}$ s for the iron electronic moments around 200 K.

Excitation with light creates two additional localized paramagnetic centers, at the special pair and at the primary quinone Q_A. The correlation time of the magnetic moment associated with $P^{\bullet+}$ should be of the order of 1 μs (Bowman et al., 1979). The correlation time of its counterpart at $Q^{\bullet+}$, however, is much shorter, since the magnetic moment is coupled with that of the Fe^{2+}. The antiferromagnetic exchange interaction was determined with magnetic susceptibility measurements as $J/k_B \sim 0.4$ K (Butler et al., 1980, 1984), implying a flip rate of 10^{-10}–10^{-11} s^{-1}. This rapid reorientation

is also largely responsible for the broad EPR line which is only observable at temperatures below 20 K (Calvo et al., 1982; Butler, 1984).

With the formulae given under Materials and Methods, the effect of these paramagnetic moments on the T_1, T_1^ρ, and T_2 is now easily estimated. The most pronounced effects may be expected for the oxidized primary donor. Due to its relatively long relaxation time $\tau_p = 10^{-6}$ s, the CP efficiency is expected to be severely reduced (^{1}H $T_1^\rho < 1$ ms) at distances shorter than ~20 Å. At this distance, a T_2 broadening of ~20 Hz is calculated. The dipolar splitting in the rotating frame is estimated as $\omega_D = \gamma_n\gamma_p S\hbar/r^3 = 9 \times 10^3$ rad/s. Since $\tau_p^{-1} \gg \omega_D$, the T_2 broadening is in the "weak collision limit", and the dipolar field will leave the relative intensities of center band and side bands of the CP/MAS pattern essentially unaffected [see, e.g., Abragam (1961)].

For the RC in the dark, the paramagnetic Fe^{2+} with $S = 2$, an effective magnetic moment $g\sqrt{S(S+1)} = 5.85\ \mu_B$ (Butler et al., 1980), and, for instance, $\tau_p = 10^{-10}$ s is expected to give rise to broadening (^{13}C T_1, $T_2 < 10$ ms) as well as reduced cross-polarization efficiency at distances less than ~7 Å. For the exchange-coupled $Q^{\bullet-}$, with $S = {}^1/_2$, a magnetic moment $gS = 1\ \mu_B$, and a similar correlation time $\tau_p = 10^{-10}$ s, the spherical volume that is affected should be smaller, with a radius of 4–5 Å.

We are now in a position to discuss the light-induced changes in the CP/MAS spectra of the [4′-^{13}C]Tyr RCs. The bottleneck for CP/MAS around the oxidized primary donor is predicted to occur at a cutoff radius of ~20 Å, and quite a number of tyrosines are found within this range of the special pair: L128 (16 Å), L144 (10 Å), L148 (15 Å), L162 (5 Å), L169 (13 Å), and M210 (5 Å) inside the helix-shielded region, L164 (10 Å) in the periplasmic domain, and two exposed residues L67 (16 Å) and L144 (10 Å) (Rees et al., 1989; Chang et al., 1991). In parentheses the approximate distance to the macroaromatic cycles of the special pair is given. On the other hand, there are no tyrosine labels within the T_1 broadening range for the paramagnetic centers at the cytoplasmic side of the complex (Rees et al., 1989; Chang et al., 1991). The nearest tyrosine for both Fe and Q_A is H40, with its label at 15 Å from the Fe and ~7 Å from the Q_A. There are no tyrosine labels close to the secondary quinone also. The nearest one is L222, with its label at a distance of ~9 Å. Light-induced differences for the tyrosine signals should therefore be associated with tyrosines located in the environment of the oxidized primary donor.

The theoretical considerations above predict a partial collapse of the NMR signal due to a short T_1^ρ for labels in the vicinity of the $P^{\bullet+}$ paramagnetic radical. In Figure 8A the spectrum for the illuminated sample is therefore scaled onto the data for the RC in the dark in such a way that there is only a decrease of the signal intensity upon excitation with light. Then the two signals coincide at the downfield side of the peak.[4] Figure 8 panels B and C contain the first- and second-derivative spectra, with the same relative scaling of the two traces as in Figure 8A. It appears that three of the four narrow signals that dominate the second-derivative spectra are substantially reduced after illumination of the sample. This includes the two narrowest resonances at 152.2 and 155.7 ppm. Therefore the surrounding of the special pair is the most rigid and well-defined part of the protein as probed by the tyrosines. This is in qualitative agreement with inferences from the molecular dynamics simulations of the transmembrane region of the homologous RC complex of *R. viridis* (Treutlein et al., 1988a, 1992). In addition, the data provide strong evidence that the surrounding of the special pair is unique. This is of importance since the broad absorption spectrum of P is often taken as evidence for a glassy, heterogeneous environment, as opposed to the ordered surrounding that transpires from the NMR.

Electrostatic Differences Probed with the Tyrosine Labels. It is perhaps surprising that the range of isotropic shifts observed for the labels (152.2–157.3 ppm) is not excessive compared to what has been found in various other proteins, in a membrane (Herzfeld et al., 1990; McDermott et al., 1991) or in solution (Maurer et al., 1974). The 4′ position in the phenolic side chain of the tyrosine provides a sensitive probe for electrostatic effects in the protein that influence the local electron density or polarization of the aromatic side chain. The effect of such charge density variations on carbon chemical shifts in aromatic and conjugated systems is approximately +155 ppm shift per positive electronic equivalent (Spiesecke & Schneider, 1961; Tokuhiro & Fraenkel, 1969; Strub et al., 1983). The center-band resonance of the label extends over ~5 ppm in total (cf. Figure 3), which translates into a local charge variation of not more than ~0.03 electronic equivalent between the various tyrosines observed in our CP/MAS spectra. The NMR data therefore provide evidence for a rather uniform protein complex, without any substantial electrostatic effects at individual tyrosines associated with charge transfer, polarization by a nearby charge, or deprotonation of the tyrosine side chain. For instance, deprotonated tyrosines should give rise to signals in between 165 and 167 ppm (Herzfeld et al., 1990). Furthermore the transmembrane helices are expected to give rise to large dipole moments of ~50 D (Hol et al., 1981). Although the electrostatic fields associated with the helix dipoles should largely cancel due to their antiparallel arrangement, it has been suggested that strong interactions may exist between individual side chains and α-helix dipoles (Hol et al., 1981). The NMR results do not reveal any evidence for strong electric dipole interactions involving phenolic tyrosine side chains.

Most of the signal from the label is divided over two broader components. The experiments at different temperatures suggest that the downfield component, which includes the additional intensity that is established when cooling the sample, is mainly associated with residues in polar sections of the complex. On the other hand, the upfield component is associated with residues in the more rigid sections of the complex, which should be predominantly apolar (Rees et al., 1989; Chang et al., 1991). Therefore the difference in chemical shift between the two broader signals probably reflects global electrostatic or thermodynamic differences between the polar and apolar regions of the RC, for instance due to changes in hydrogen-bonding environment around the phenolic oxygen. The same conclusion was reached in the earlier work based on chemical shift considerations (de Groot et al., 1990a). The shift difference amounts to 1.2 ppm, which translates into ~0.01 electronic equivalent. This suggests that global electrostatic variations associated with the differences between the polar and apolar sections of the complex are small compared to the local electrostatic variations around individual residues.

Quite a number of tyrosine phenolic side chains are thought to be of importance for the efficient operation of the RC. For instance, two, M210 and L162, contribute to the breaking of the near-2-fold symmetry and are part of the aromatic

[4] Note that the light-induced changes cannot be explained by sample heating associated with the illumination. With scaling as in Figure 8A, heating would yield a coincidence of the *upfield* sides of the tyrosine signals (see also Figure 3).

environment in the immediate vicinity of the special pair. L162 is conserved and may be involved in the rereduction of the special pair since it is located between the dimer and the putative cytochrome heme binding site (Rees et al., 1989; Chang et al., 1991). Tyrosine M210, which is also conserved between several different purple species [see, e.g., Komiya et al. (1988)], has attracted the most attention, and site-directed mutagenesis studies on RC of various organisms have provided evidence that it is of importance for the fast rate of the primary electron transfer (Finkele et al., 1990; Nagarajan et al., 1990; Chan et al., 1991). Also, L169 and M199 are conserved between different species, as well as L222, which is located in the Q_B binding domain and may play a role in proton transport to the quinone acceptors (Komiya et al., 1988; Takahashi et al., 1990).

Mutagenesis studies have provided strong evidence that none of the tyrosines mentioned above is a prerequisite for the function of the RC, since tyrosine point mutations only give rise to relatively small changes of the efficiency of the RC (Farchaus et al., 1990; Finkele et al., 1990; Nagarajan et al., 1990; Chan et al., 1991). Multiple modifications are necessary to render the RC photosynthetically inactive (Robles et al., 1990). Along the same line, the NMR suggests that, provided electrostatic motifs involving tyrosines are essential for the photochemistry, they should extend over more than one amino acid. For instance, it is difficult to imagine that M210 would be of crucial importance for the symmetry breaking and force the electron transfer over the A branch only, without a considerable polarization of its aromatic side chain and a corresponding shift in the ^{13}C NMR spectrum. One possibility that is not excluded by our data is an asymmetry due to the presence of certain amino acids, including the tyrosines. This has been suggested as one of the factors that is of importance for the fast electron transport and the asymmetry of electron transfer with respect to the two branches (Yeates et al., 1987; Creighton et al., 1988; Treutlein et al., 1988b; Chan et al., 1991).

CONCLUSION

Proteins are generally thought of as subject to diffusive motions governed by thermal fluctuations that mediate transitions between different conformational substates different from the average structure (Cooper, 1976; Brooks et al., 1988). CP/MAS studies in the light and in the dark at various temperatures, and study of the relaxation properties, provide converging evidence that between 215 and 265 K the immediate environment of the special pair is extremely well-defined, static on the NMR time scale, and rigid. The lack of homogeneous and inhomogeneous broadening beyond the intrinsic resolution of the CP/MAS experiment over the entire temperature range for the narrow resonances strongly suggests that deviations from the average structure for the environment of the special pair are also small at physiological temperatures.

An important point of interest is whether conformational distortions, possibly involving one or more tyrosines, occur upon excitation with light, in particular in the surrounding of the special pair. Some inferences can be made using the NMR data in the dark-adapted state. The data suggest a firm interior that is not likely to react easily on the time scale of the primary photoprocess. To illustrate this point, we calculate the dissipation energy E_d for the displacement of a sphere with radius r over a distance r in a viscous medium with viscosity η_i, which is, according to Stoke's law, expressed as $E_d = 6\pi\eta_i r^3/\tau$. Hence for $\eta_i > 10^5$ Pa·s the conformational changes on the time scale of the first stages of the primary photo process, τ = 3–5 ps (Fleming et al., 1988), should be negligible, even if a substantial part of the photon energy would be dissipated. This questions a dominant role for conformational changes other than small and probably elastic nuclear displacements in the first stages of the primary photoprocess and may be of importance for efficient electron transport in the primary reaction. It is corroborated by at least two other experimental observations: The rate of the primary reaction in RC complexes does not vary substantially between helium temperatures and room temperature (Fleming et al., 1988), and recent resonance Raman studies of wild-type RCs and complexes mutated at Tyr M210 did not provide any evidence for structural changes upon mutation, indicating a firm immediate environment of the special pair largely withstanding the effect of the mutation (Mattioli et al., 1991). The tolerance of the viscosity argument is quite good: even a displacement of a group the size of a phenolic side chain through a viscous medium over ~1 Å on the time scale of the $P^{\bullet+}Q^{\bullet-}$ electron transfer, $\tau \sim 200$ ps (Parson, 1968), would require $\eta_i \sim 10$ Pa·s, orders of magnitude lower than the limiting value extracted from the NMR data and in the range where pronounced effects on the ^{13}C shift tensor and the CP/MAS efficiency are expected, comparable to those for the detergent at the higher temperatures. The present results therefore support recent evidence that the primary reaction $PQ \rightarrow P^{\bullet+}Q^{\bullet-}$ may be not coupled to low-frequency protein motions (Gunner & Dutton, 1988; Moser et al., 1992). In this respect, we note that the strongest evidence in favor of protein conformational distortions has been from optical hole-burning experiments, which show coupling to low-frequency (<200 cm$^{-1} = 6 \times 10^{12}$ Hz) motions during the primary process (Johnson et al., 1991). It was tacitly assumed that these soft modes were associated with the protein surrounding and were involved in ultrafast vibrational cooling by energy dissipation into the protein (Johnson et al., 1990). This interpretation was reviewed when rapid flow Resonance Raman experiments revealed large displacements in only a few well-defined Raman active modes at 36, 71, 94, and 127 cm^{-1} *in the special pair* that may be associated with motions of the metal or in and out of plane deformations (Shreve et al., 1991; Lutz & Mäntele, 1991). Interestingly, such modes are not observed with Raman excitation resonant with the monomeric chlorophylls. In addition, it was found that, with applied electric fields and for mutants with different ΔG, the rates of primary charge separation were only moderately affected (Lockhart et al., 1990; Kirmaier et al., 1991; Woodbury et al., 1990). This led Middendorf et al. (1991) to propose an alternative interpretation for their hole-burning experiments. They stated that parallel transfer with similar rates from a set of vibrational levels could also explain the hole-burning data (Jortner, 1980), provided that the crossing of the potential energy surface of the primary donor and acceptor is near the minimum of the donor surface. It is evident that the NMR results provide additional support for such a scheme. A linear elastic protein environment may assist in preventing vibrational relaxation, while the extremely rigid and well-defined structure that transpires from the NMR may be necessary for an exact positioning of the prosthetic groups in order to obtain an appropriate energy surface crossing and a precise deformation of the special pair already in the ground state, as evidenced

[5] Ring current shifts were estimated using the Johnson–Bovey (1958) model, with eq 9 and 10 in Janson and Katz (1979), where we have used $a = 4.78$ Å as the radius of the current loop, $n = 4.31$, the effective number of electrons in the loop, and $2\rho = 1.28$ Å, the separation of the loops (Janson et al., 1969).

by the limited set of well-defined modes found in the Raman spectrum.

The range of chemical shifts is too small to interpret the dispersion in terms of variations in chemical environment for individual residues. The present data only lead to a *tentative* and *preliminary* assignment of the signal from the M210 residue, in between the special pair and B_A, at 152.2 ppm. M210 is expected to resonate upfield for three reasons: (i) According to the X-ray data, M210 is located above the macroaromatic cycles of B_A and the primary donor and should be subject to an estimated upfield ring current shift of $\sim$1.4 ppm.[5] (ii) M210 is located deep inside the apolar region, and (iii) it is probably not hydrogen bonded at the phenolic oxygen (Mattioli et al., 1991; Chang et al., 1991). In addition, M210 is in the immediate environment of the primary donor, and therefore its NMR signal is expected to be among the narrow signals that are suppressed in the presence of the light-induced electronic moment at the primary donor (cf. Figure 8C). In order to obtain definite assignments for particular signals, additional NMR experiments involving site-specific mutations of labeled protein complexes are in progress.

ACKNOWLEDGMENT

We thank A. H. M. de Wit, A. H. H. van Houten, and S. J. Jansen for culturing the cells and isolating the reaction centers and C. Erkelens for his assistance with the NMR apparatus. We acknowledge S. Völker for helpful and critical discussions on the hole-burning topic. The two coordinate sets of *R. sphaeroides* RC were kindly provided to us by G. Feher and M. Schiffer.

REFERENCES

Abragam, A. (1961) *The Principles of Nuclear Magnetism*, Oxford University Press, London.

Abrahams, J. P. (1991) Thesis, University of Leiden, The Netherlands.

Allen, P. J., Creuzet, F., de Groot, H. J. M., & Griffin, R. G. (1991) *J. Magn. Reson. 92*, 614–617.

Boso, J., Debrunner, P., Okamura, M. Y., & Feher, G. (1981) *Biochim. Biophys. Acta 638*, 173–177.

Bowman, M. K., Norris, J. R., & Wraight, C. A. (1979) *Biophys. J. 25*, 203a.

Brooks, C. L., Karplus, M., & Montgomery Pettitt (1988) in *Proteins: A Theoretical Perspective of Dynamics, Structure and Thermodynamics, Advances in Chemical Physics LXXI* (Prigogine, I., & Riu, S. A., Eds.) Wiley, New York.

Butler, W. F., Johnston, D. C., Shore, H. B., Fredkin, D. R., Okamura, M. Y., & Feher, G. (1980) *Biophys. J. 32*, 967–992.

Butler, W. F., Calvo, R., Fredkin, D. R., Isaacson, R. A., Okamura, M. Y., & Feher, G. (1984) *Biophys. J. 45*, 947–973.

Calvo, R., Butler, W. F., Isaacson, R. A., Okamura, M. Y., Fredkin, D. R., & Feher, G. (1982) *Biophys. J. 37*, 111a.

Campbell, I. D., Dobson, C. M., Moore, G. R., Perkins, S. J., & Williams, R. J. P. (1976) *FEBS Lett. 70*, 96–100.

Chan, C.-K., Chen, L. X.-Q., DiMagno, T. J., Hanson, D., Nance, S. L., Schiffer, M., Norris, J. R., & Fleming, G. R. (1991) *Chem. Phys. Lett. 176*, 366–372.

Chang, C.-H., El-Kabbani, O., Tiede, D., Norris, J., & Schiffer, M. (1991) *Biochemistry 30*, 5352–5360.

Cooper, A. (1976) *Proc. Natl. Acad. Sci. U.S.A. 73*, 2740–2741.

Creighton, S., Hwang, J.-K., Warshel, A., Parson, W. W., & Norris, J. (1988) *Biochemistry 27*, 774–781.

Debrunner, P. G., Schulz, C. E., Feher, G., & Okamura, M. Y. (1975) *Biophys. J. 15*, 226a.

de Groot, H. J. M. (1986) Thesis, Leiden University.

de Groot, H. J. M., de Jongh, L. J., ElMassalami, M., Thiel, R. C., & Smit, H. H. A. (1986) *Hyperfine Interact. 27*, 93–110.

de Groot, H. J. M., Copié, V., Smith, S. O., Allen, P. J., Winkel, C., Lugtenburg, J., Herzfeld, J., & Griffin, R. G. (1988) *J. Magn. Reson. 77*, 251–257.

de Groot, H. J. M., Raap, J., Winkel, C., Hoff, A. J., & Lugtenburg, J. (1990a) *Chem. Phys. Lett. 169*, 307–310.

de Groot, H. J. M., Smith, S. O., Courtin, J. M. L., van den Berg, E., Winkel, C., Lugtenburg, J., Griffin, J., & Herzfeld, J. (1990b) *Biochemistry 29*, 6873–6883.

de Groot, H. J. M., Smith, S. O., Kolbert, A. C., Courtin, J. M. L., Winkel, C., Lugtenburg, J., Herzfeld, J., & Griffin, J. (1991) *J. Magn. Reson. 91*, 30–38.

Deisenhofer, J., & Michel, H. (1989) *EMBO J. 8*, 2149–2170.

Devreux, F., Boucher, J.-P., & Nechtschein, M. (1974) *J. Phys. (Paris) 35*, 271–285.

Farchaus, J. W., Wachtveitl, J., Mathis, P., & Oesterhelt, D. (1990) in *Current Research in Photosynthesis, Proceedings of the VIIIth Congress on Photosynthesis, Stockholm 1989* (Baltscheffsky, M., Ed.) Vol. I, pp I.1.197–I.1.201, Kluwer, the Netherlands.

Feher, G., & Okamura, M. Y. (1978) in *The Photosynthetic Bacteria* (Clayton, R. K., & Sistrom, W. R., Eds.) pp 349–386, Plenum Press, New York.

Feher, G., Hoff, A. J., Isaacson, R. A., & Ackerson, L. C. (1975) *Ann. N.Y. Acad. Sci. 244*, 239–259.

Finkele, U., Lauterwasser, C., Zinth, W., Gray, K. A., & Oesterhelt, D. (1990) *Biochemistry 29*, 8517–8521.

Fischer, K. A., & Stoeckenius, W. (1983) in *Biophysics* (Hoppe, W., Lohmann, W., Markl, H., & Ziegler, H., Eds.) p 417, Springer-Verlag, Berlin.

Fleming, G. R., Martin, J. L., & Breton, J. (1988) *Nature 333*, 190–192.

Frauenfelder, H., & Wolynes, P. G. (1985) *Science 229*, 337–345.

Friesner, R. A., & Won, Y. (1989) *Biochim. Biophys. Acta 977*, 99–122.

Gephard, R., van der Hoef, K., Violette, C. A., de Groot, H. J. M., Frank, H. A., & Lugtenburg, J. (1991) *Pure Appl. Chem. 63*, 115–122.

Griffin, R. G., Aue, W. P., Haberkorn, R. A., Harbison, G. S., Herzfeld, J., Menger, E. M., Munowitz, M. G., Olejniczak, E. T., Raleigh, D. P., Roberts, J. E., Ruben, D. J., Schmidt, A., Smith, S. O., & Vega, S. (1988a) in *Physics of NMR Spectroscopy in Biology and Medicine*, Proceedings of the Enrico Fermi International School of Physics, July 8–18, 1986, Varenna, Italy, North Holland Press, Amsterdam.

Griffin, R. G., Beshah, K., Ebelhäuser, R., Huang, T. H., Olejniczak, E. T., Rice, D. M., Siminovitch, D. J., & Wittebort, R. J. (1988b) in *The Time Domain in Surface and Structural Dynamics* (Long, G. J., & Grandjean, Eds.) pp 81–105, Kluwer, The Netherlands.

Gunner, M. R., & Dutton, P. L. (1988) in *The Photosynthetic Bacterial Reaction Center: Structure and Dynamics*, (Breton, J., & Vermèglio, A., Eds.) NATO ASI Series, Series A: Life Sciences, Vol. 149, pp 259–269, Plenum, New York.

Harbison, G. S., Smith, S. O., Pardoen, J. A., Courtin, J. M. L., Lugtenburg, J., Herzfeld, J., Mathies, R. A., & Griffin, R. G. (1985) *Biochemistry 24*, 6955–6962.

Harbison, G. S., Roberts, J. E., Herzfeld, J., & Griffin, R. G. (1988) *J. Am. Chem. Soc. 110*, 7221–7223.

Herzfeld, J., & Berger, A. E. (1980) *J. Chem. Phys. 73*, 6021–6030.

Herzfeld, J., Das Gupta, S. K., Farrar, M. R., Harbison, G. S., McDermott, A., Pelletier, S. L., Raleigh, D. P., Smith, S. O., Winkel, C., Lugtenburg, J., & Griffin, R. G. (1990) *Biochemistry 29*, 5567–5574.

Hol, W. G. J., Halie, L. M., & Sander, C. (1981) *Nature 294*, 532–536.

Janson, T. R., & Katz, J. J. (1979) in *The Porphyrins* (Dolphin, D., Ed.) Vol. 4, pp 1–59, Academic Press, London.

Janson, T. R., Kane, A. R., Sullivan, J. F., Knox, K., & Kenney, M. E. (1969) *J. Am. Chem. Soc. 91*, 5210–5214.

Johnson, C. E., Jr., & Bovey, F. A. (1958) *J. Chem. Phys. 29*, 1012–1014.
Johnson, S. G., Tang, D., Jankowiak, R., Hayes, J. M., Small, G. J., & Tiede, D. M. (1990) *J. Phys. Chem. 94*, 5894–5855.
Johnson, S. G., Lee, I.-J., & Small, G. J. (1991) in *The Chlorophylls* (Scheer, H., Ed.) pp 739–768, CRC Press, Boca Raton, FL.
Jortner, J. (1980) *J. Am. Chem. Soc. 102*, 6676.
Kirmaier, C., Gaul, D., DeBey, R., Holten, D., & Schenk, C. C. (1991) *Science 251*, 922.
Komiya, H., Yeates, T. O., Rees, D. C., Allen, J. P., & Feher, G. (1988) *Proc. Natl. Acad. Sci. U.S.A. 85*, 7226–7230.
Lewis, B. A., Harbison, G. S., Herzfeld, J., & Griffin, R. G. (1985) *Biochemistry 24*, 4671–4679.
Lockhart, D. J., Kirmaier, C., Holten, D., & Boxer, S. G. (1990) *J. Phys. Chem. 94*, 6987.
Lowe, I. J., & Tse, D. (1968) *Phys. Rev. 166*, 279–291.
Lutz, M., & Mäntele, W. (1991) in *Chlorophylls* (Scheer, H., Ed.) pp 855–902, CRC Press, Boca Raton, FL.
Mattioli, T. A., Gray, K. A., Lutz, M., Oesterhelt, D., & Robert, B. (1991) *Biochemistry 30*, 1715–1722.
Maurer, W., Haar, W., & Rüterjans, H. (1974) *Z. Phys. Chem. 93*, 119–129.
McDermott, A. E., Thompson, L. K., Farrar, M. R., Pelletier, S., Lugtenburg, J., Herzfeld, J., & Griffin, R. G. (1991) *Biochemistry 30*, 8366–8371.
Middendorf, T. R., Mazzola, L. T., Gaul, D. F., Schenk, C. C., & Boxer, S. G. (1991) *J. Phys. Chem. 95*, 10142–10151.
Möbius, K., Lubitz, W., & Plato, M. (1989) in *Advanced EPR, Applications in Biology and Biochemistry* (Hoff, A. J., Ed.) pp 441–499, Elsevier, Amsterdam, The Netherlands.
Moser, C. C., Keske, J. M., Warncke, K., Farid, R. S., & Dutton, P. L. (1992) *Nature 355*, 796–802.
Nagarajan, V., Parson, W. W., Gaul, D., & Schenk, C. (1990) *Proc. Natl. Acad. Sci. U.S.A. 87*, 7888–7892.
Parak, F., Fischer, M., Heidemeier, J., Engelhard, M., Kohl, K.-D., Hess, B., & Formanek, H. (1990) *Hyperf. Int. 58*, 2381–2385.
Parson, W. W. (1968) *Biochim. Biophys. Acta 153*, 248–259.
Parson, W. W., Warshel, A., Creighton, S., & Norris, J. (1988) in *The Photosynthetic Bacterial Reaction Center: Structure and Dynamics* (Breton, J., & Verméglio, A., Eds.) NATO ASI Series, Series A: Life Sciences Vol. 149, pp 309–317, Plenum, New York.
Parson, W. W., Chu, Z.-T., & Warshel, A. (1990) *Biochim. Biophys. Acta 1017*, 251–272.
Pausak, S., Pines, A., & Waugh, J. S. (1973) *J. Chem. Phys. 59*, 591–595.
Philippoff, W., & Gaskins, F. H. (1956) *J. Polym. Sci. 31*, 205–211.
Raap, J., Winkel, C., de Wit, A. H. M., van Houten, A. H. H., Hoff, A. J., & Lugtenburg, J. (1990) *Anal. Biochem. 191*, 9–15.
Rees, D. C., Komiya, H., Yeates, T. O., Allen, J. P., & Feher, G. (1989) *Annu. Rev. Biochem. 58*, 607–633.
Robles, S. J., Breton, J., & Youvan, D. C. (1990) *Science 248*, 1402–1405.
Roth, M., Lewit-Bentley, A., Michel, H., & Deisenhofer, J. (1989) *Nature 340*, 659–661.
Shreve, A. P., Cherepy, N. J., Franzen, S., Boxer, S. G., & Mathies, R. A. (1991) *Proc. Natl. Acad. Sci. U.S.A. 88*, 11207–11211.
Smith, S. O., & Griffin, R. G. (1988) *Annu. Rev. Phys. Chem. 39*, 511–535.
Smith, S. O., de Groot, H. J. M., Gebhard, R., Courtin, J. M. L., Lugtenburg, J., Herzfeld, J., & Griffin, R. G. (1989) *Biochemistry 28*, 8897–8904.
Smith, S. O., Courtin, J. M. L., de Groot, H. J. M., Gebhard, R., & Lugtenburg, J. (1991) *Biochemistry 30*, 7409–7415.
Spiesecke, J., & Schneider, W. G. (1961) *Tetrahedron Lett. 14*, 468–472.
Strub, H., Beeler, A. J., Grant, D. M., Michl, J., Cutts, P. W., & Zilm, K. (1983) *J. Am. Chem. Soc. 105*, 3333–3334.
Suwelack, D., Rothwell, W. P., & Waugh, J. S. (1980) *J. Chem. Phys. 73*, 2559–2569.
Takahashi, E., Maroti, P., & Wraight, C. A. (1990) in *Current Research in Photosynthesis, Proceedings of the VIIIth Congress on Photosynthesis, Stockholm 1989* (Baltscheffsky, M., Ed.) Vol. I, pp I.1.169–I.1.172, Kluwer, The Netherlands.
Tegenfelt, J., & Haeberlen, U. (1979) *J. Magn. Reson. 36*, 453–457.
Treutlein, H., Schulten, K., Deisenhofer, J., Michel, H., Brünger, A., & Karplus, M. (1988a) in *The Photosynthesis Bacterial Reaction Center* (Breton, J., & Verméglio, A., Eds.) NATO ASI Series A, Vol. 149, pp 139–150, Plenum Press, New York.
Treutlein, H., Schulten, K., Niedermeier, C., Deisenhofer, J., Michel, H., & DeVault D. (1988b) in *The Photosynthesis Bacterial Reaction Center* (Breton, J., & Verméglio, A., Eds.) NATO ASI Series A, Vol. 149, pp 369–377, Plenum Press, New York.
Treutlein, H., Schulten, K., Brünger, A. T., Karplus, M., Deisenhofer, J., & Michel, H. (1992) *Proc. Natl. Acad. Sci. U.S.A. 89*, 75–79.
Tokohiru, T., & Fraenkel, G. (1969) *J. Am. Chem. Soc. 91*, 5005–5013.
Van Wazer, J. R., Lyons, J. W., Kim, K. Y., & Colwell, R. E. (1963) in *Viscosity and Flow Measurement, A Laboratory Handbook of Rheology*, Wiley, New York.
Veeman, W. S. (1984) *Prog. Nucl. Magn. Reson Spectrosc. 16*, 193–235.
Warshel, A., Chu, Z.-T., & Parson, W. W. (1989) *Science 246*, 112–116.
Weast, R. C., & Astle, M. J., Eds. (1980) *CRC Handbook of Chemistry and Physics*, 60th ed., pp F-52–F-57, CRC Press, Boca Raton, FL.
Williams, J. C., Steiner, L. A., & Feher, G. (1986) *Proteins: Struct., Funct., Genet. 1*, 312–325.
Winkel, C., Aarts, M. W. M. M., van der Heide, F. R., Buitenhuis, E. G., & Lugtenburg, J. (1989) *Recl. Trav. Chim. Pays-Bas 108*, 139–146.
Woodbury, N. W., Taguchi, A. K., Stocker, J. S., & Boxer, S. G. (1990) in *Reaction Centers of Photosynthetic Bacteria* (Michel-Beyerle, M.-E., Ed.) p 303, Springer, Berlin.
Yeates, T. O., Komiya, H., Rees, D. C., Allen, J. P., & Feher, G. (1987) *Proc. Natl. Acad. Sci. U.S.A. 84*, 6438–6442.
Zager, S. A., & Freed, J. H. (1982) *J. Chem. Phys. 77*, 3360–3375.